IOP PUBLISHING PHYSICS IN MEDICINE AND BIOLOGY

Phys. Med. Biol. **55** (2010) 5817–5831 doi:10.1088/0031-9155/55/19/013

Development of a Si-PM-based high-resolution PET system for small animals

Seiichi Yamamoto[1,4], Masao Imaizumi[2], Tadashi Watabe[2], Hiroshi Watabe[3], Yasukazu Kanai[3], Eku Shimosegawa[2] and Jun Hatazawa[2,3]

[1] Kobe City College of Technology, Kobe, Japan
[2] Department of Nuclear Medicine and Tracer Kinetics, Osaka University Graduate School of Medicine, Osaka, Japan
[3] Department of Molecular Imaging in Medicine, Osaka University Graduate School of Medicine, Osaka, Japan

E-mail: s-yama@kobe-kosen.ac.jp

Received 19 June 2010, in final form 17 August 2010
Published 16 September 2010
Online at stacks.iop.org/PMB/55/5817

Abstract

A Geiger-mode avalanche photodiode (Si-PM) is a promising photodetector for PET, especially for use in a magnetic resonance imaging (MRI) system, because it has high gain and is less sensitive to a static magnetic field. We developed a Si-PM-based depth-of-interaction (DOI) PET system for small animals. Hamamatsu 4 × 4 Si-PM arrays (S11065-025P) were used for its detector blocks. Two types of LGSO scintillator of 0.75 mol% Ce (decay time: ~45 ns; 1.1 mm × 1.2 mm × 5 mm) and 0.025 mol% Ce (decay time: ~31 ns; 1.1 mm × 1.2 mm × 6 mm) were optically coupled in the DOI direction to form a DOI detector, arranged in a 11 × 9 matrix, and optically coupled to the Si-PM array. Pulse shape analysis was used for the DOI detection of these two types of LGSOs. Sixteen detector blocks were arranged in a 68 mm diameter ring to form the PET system. Spatial resolution was 1.6 mm FWHM and sensitivity was 0.6% at the center of the field of view. High-resolution mouse and rat images were successfully obtained using the PET system. We confirmed that the developed Si-PM-based PET system is promising for molecular imaging research.

(Some figures in this article are in colour only in the electronic version)

1. Introduction

Simultaneous measurement of PET and MRI is a promising strategy for the molecular imaging field. The advantage of PET is its ability to image the radionuclide with high detection

[4] Author to whom any correspondence should be addressed.

0031-9155/10/195817+15$30.00

sensitivity. MRI can provide high-resolution anatomical images with a large variety of tissue contrast. Such functional information as diffusion, magnetic resonance spectroscopy (MRS), or functional MRI (fMRI) can also be obtained with a high magnetic field MRI. In addition, a PET/MRI combined system can simultaneously measure a subject. It minimizes registration errors and reduces the imaging time for PET and MRI.

For a long time, photomultiplier tubes (PMTs) have been used for major photodetectors for PET systems because of their high gain, low noise, high speed response, excellent stability and relatively low cost. Position-sensitive PMTs (PSPMTs) are also used for small animal PET systems. However, PMTs and PSPMTs are sensitive to magnetic fields complicating their use near or inside magnetic resonance imaging (MRI) systems. The height of a PMT is relatively large, and the diameter of the PET detector ring also becomes large, which makes it difficult to be used in narrow MRI tunnels. Consequently, PMTs or PSPMTs are basically not good candidates for PET/MRI combined systems. To solve these problems, using optical fibers between scintillators and PSPMTs was proposed for PET/MRI combined systems and several MR-compatible PET inserts and PET/MRI systems were developed (Shao *et al* 1997a, 1997b, Garlick *et al* 1997, Raylman *et al* 2006, Slate *et al* 1999, Yamamoto and Murayama 2005, Yamamoto *et al* 2009, 2010). In these systems, only the scintillators were positioned inside the MRI, and the scintillation photons were transferred outside the magnet where the magnetic field was low enough to use PSPMTs. In these systems, although no interference between PET and MRI was observed, the light loss due to the fibers was more than 70%, and the cost of fibers was also significant. In other approaches, avalanche photodiode (APD) and position-sensitive APD-based PET detectors have been used for PET inserts for PET/MRI combined systems (Pichler *et al* 2006, Judenhofer *et al* 2008, Catana *et al* 2006, 2008). However, these photosensors need high-cost application-specific integrated circuits (ASIC) because of their relatively low gain.

The Geiger-mode avalanche photodiode is a newly developed silicon-based photodetector that is also called a silicon photomultiplier (Si-PM) (Ottea *et al* 2005, Finocchiaro *et al* 2009). It is a photon-counting device consists of multiple APD pixels operating in Geiger mode. Since Si-PM is less sensitive to static magnetic fields (Hong *et al* 2008) and its height is small similar to APD, it is a promising candidate for the photodetector for PET/MRI combined systems. Compared to APD, the gain of Si-PM is much higher, and thus it is easy to use, and its timing property combined with a fast scintillator is excellent (Schaart *et al* 2010). However, a Si-PM-based PET system has not been yet reported although some block detector designs have been reported (Schaart *et al* 2009, Kolb *et al* 2010, Llosáa *et al* 2009a, Llosa *et al* 2009b, 2009c, Cuddy *et al* 2010, Henseler *et al* 2009). We developed a Si-PM-based PET system that is compact, and no electronics circuit was positioned near the detector ring for future tests in MRI. In this paper, we describe the system and the basic performance of the developed Si-PM-based PET system measured outside MRI.

2. Materials and methods

2.1. Si-PM-based block detector

Figure 1(A) shows a photograph of the Si-PM array used for the block detector for the PET system. Hamamatsu 4 × 4 Si-PM arrays (S11064-025P) were used because they have good uniformity and temporal response, so they can also be used for a DOI detector based on pulse shape analysis. The Si-PM array has 4 × 4 channels whose size is 3 mm × 3 mm. The number of pixels per channel is 14 400. The specifications of the Si-PM are summarized in table 1.

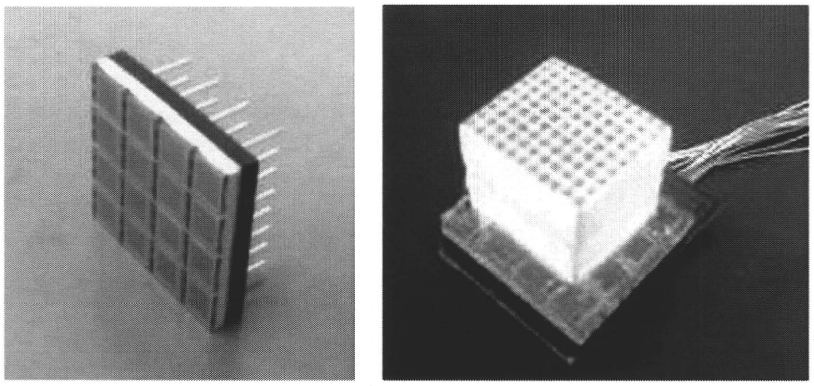

(A) (B)

Figure 1. Photograph of the Si-PM array (A) and Si-PM array-based LGSO dual-layer DOI block detector (B).

Table 1. Specification of Si-PM used for the detector block for PET.

Number of channels	16 (4 × 4)
Effective active area/channel	3 mm × 3 mm
Number of pixels/channel	14 400
Pixel size	25 μm × 25 μm
Fill factor (ratio of the active area of pixel to the entire area of pixel)	30.8
Spectral response range	320–900 nm
Operating voltage range	70 ± 10 V
Gain	2.75×10^5

The total size of the Si-PM array is 18.2 mm × 16.0 mm. Its thickness is 3.3 mm without its pin height.

To realize a DOI block detector, we selected two types of Ce-doped LGSO scintillators with different decay times (Hitachi Chemical Co., Ibaragi, Japan). LGSO has high light output similar to LSO or LYSO, and the decay time can be controlled by changing its Ce concentration (Shimizu *et al* 2006). Two types of LGSO scintillator of 0.75 mol% Ce (decay time: ~45 ns; 1.1 mm × 1.2 mm × 5 mm) and 0.025 mol% Ce (decay time: ~31 ns; 1.1 mm × 1.2 mm × 6 mm) were selected and optically coupled in the depth direction to form a DOI detector, arranged in an 11 × 9 matrix and optically coupled to the Si-PM array with a 1 mm thick light guide. The size of the LGSO block was 13.2 mm (transaxial direction) × 11.7 mm (axial direction) × 11 mm (depth). The light guide was made of acrylic resin and was used to distribute the light photon among Si-PM channels to obtain a uniform two-dimensional histogram for the block detector. For the reflector between the LGSO scintillators, 0.1 mm thick $BaSO_4$ was used (Yanagida *et al* 2009). The fabrication for the LGSO blocks with the reflectors was performed by the manufacturer (Furukawa Machines and Metals Co., Ibaragi, Japan). The fabricated Si-PM-based DOI detector without a top reflector is shown in figure 1(B).

The Si-PM array was mounted on a printed board, and the signal from each channel of the Si-PM was transferred to front-end electronics (weighted summing board). No electronics part

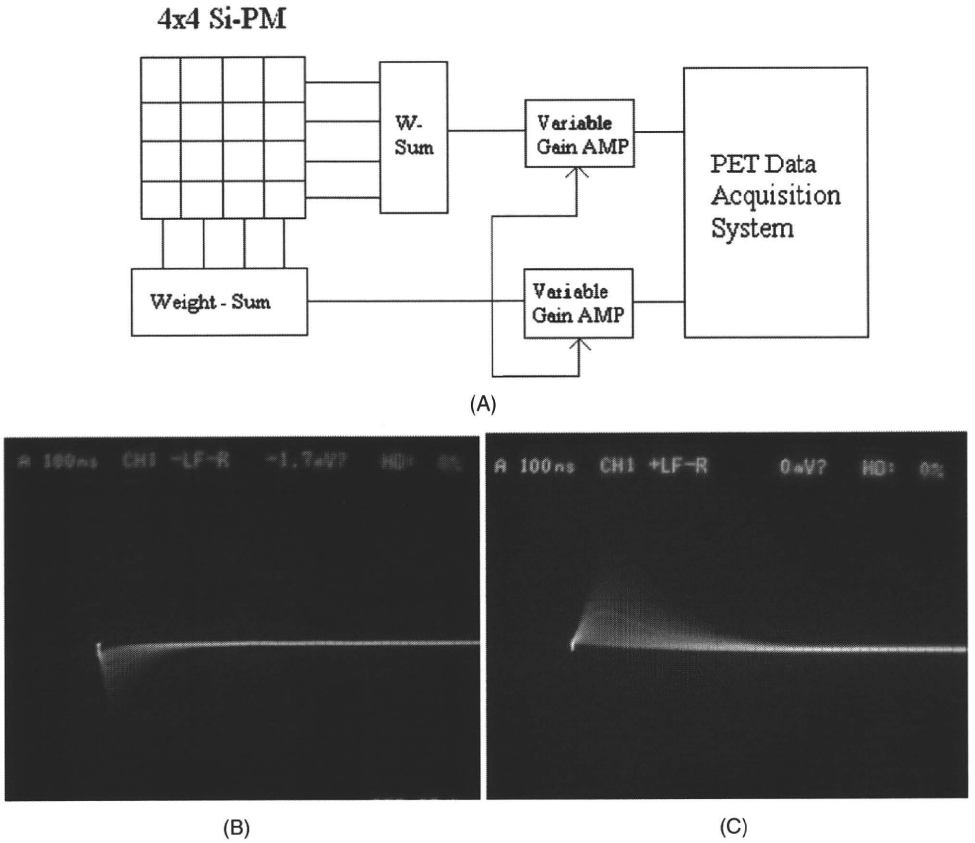

Figure 2. Block diagram of the front-end electronics used for the Si-PM PET system (A), pulse shape of one input signals from one Si-PM array (B) and one weighted sum signal at the output of the weighted sum board (B). Scales of the horizontal axis for both (A) and (B) are 100 ns per division.

is close to the block detector except a small coaxial cable connector and a capacitor to reduce the size of the detector ring of the PET system and for future tests of its MR compatibility.

A block diagram of one channel of the front-end electronics is shown in figure 2(A). The current signals from each block detector are transferred to a weighted summing board by 1.2 m long small diameter coaxial cables, terminated by 25 Ω registers and converted to voltage signals. The voltage signals are individually amplified by voltage feedback high-speed (bandwidth: 300 MHz; slew rate: 1400 V μs^{-1}) operational amplifiers (AD 8056, Analog Devices) and summed for rows and columns using summing amplifiers. These signals are weighted summed with position-dependent linear gains for each row and column to produce weighted sum signals. The weighted sum signals are transferred to the data acquisition system through variable gain amplifiers, which are prepared for the future use for the temperature-dependent gain compensation of the Si-PM arrays. The pulse shape of one input signal from the Si-PM array is shown in figure 2(B), and one weighted sum signal at the output of the weighted sum board is shown in figure 2(C). The typical rise time of the input signals for weighted summing board is 20 ns and that for the weighted summed signals is approximately 50 ns.

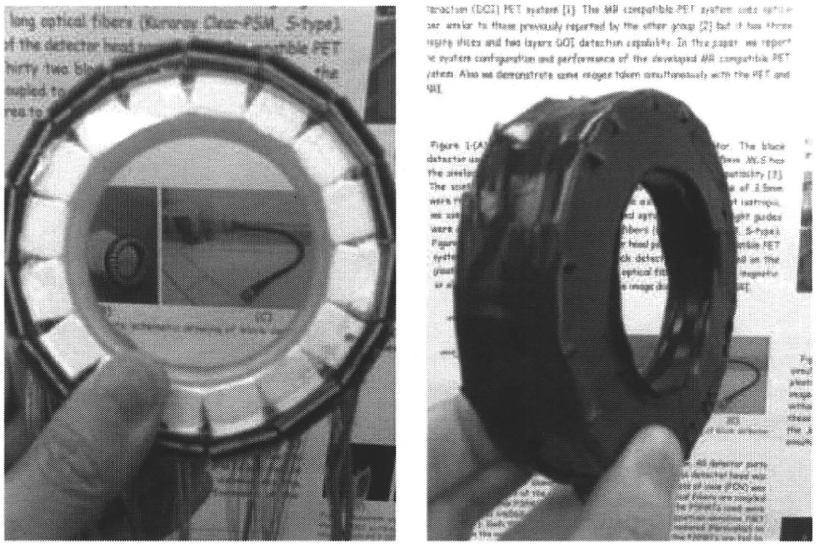

(A) (B)

Figure 3. Photograph of the PET detector ring using Si-PM-based block detectors without (A) and with a light shield (B).

Table 2. Design parameter of Si-PM PET.

Number of block detectors	16
Ring diameter	68 mm
Axial field of view	11.7 mm
Number of slices	17

2.2. Si-PM-based PET system

2.2.1. Detector ring. We developed 16 Si-PM-based block detectors and arranged them in a 68 mm inner diameter plastic ring to form the PET system. Table 2 summarizes the design parameters of the developed PET system, and figure 3 shows photographs of the developed detector ring without a light shield (A) and with a light shield (B). Although the LGSO block size of the transaxial direction (13.2 mm) is smaller than the Si-PM array size (18.2 mm), there is no gap between the top of the block detectors because they are arranged in a small diameter (68 mm). However, this will be a problem if we use the block detector for a PET system with larger diameter. The light shield was made using a black tape. The outside dimensions of the detector ring were 11 cm diameter and 2 cm thickness, and it weighs 200 g without 4 mm thick tungsten contained rubber-based end-shields and 600 g with them.

2.2.2. Data acquisition system. The weighed sum signals are fed to 100 MHz analog-to-digital (A-D) converters of the data acquisition system and integrated with two different integration times (120 ns and 320 ns) (Yamamoto 2008), and the position is calculated using the Anger principle and pulse shape discrimination by FPGA. Coincidence was also measured digitally among the eight groups (two block detectors for one group).

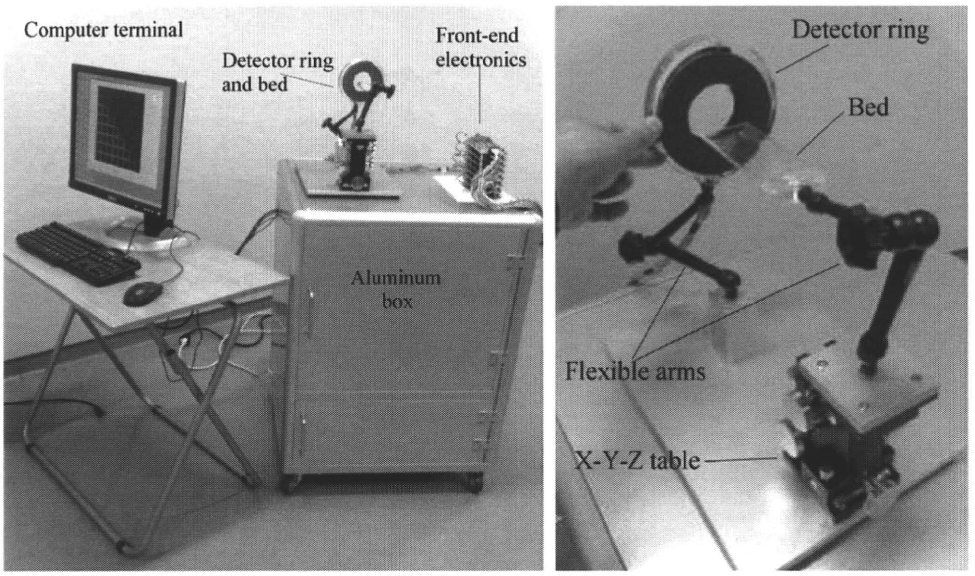

Figure 4. Photograph of the whole of the Si-PM-based PET (A) and magnified photograph of the detector ring and bed part (B).

Coincidence was measured based on the digital coincidence method, and the time window was set to 16 ns because the timing resolution of the system was around 7–8 ns, which is mainly determined by the timing property of the data acquisition system (Yamamoto *et al* 2009, 2010). Delayed coincidence was also digitally measured for the correction of the accidental events, which were subtracted in the sorting process. Coincidence events are transferred to the personal computer in the list mode. The acquired data are sorted into sinogram and reconstructed using the filtered backprojection algorithm.

2.2.3. Whole PET system. A photograph of the whole view of a Si-PM-based PET is shown in figure 4(A). The system consists of a detector ring, a bed, a front-end electronics, a computer terminal and an aluminum box in which the bias voltage supply, the data acquisition system and the personal computer were contained. A magnified photograph of the detector ring and the bed part is shown in figure 4(B). The Si-PM-based PET detector ring is supported by a plastic ring that is connected to a flexible arm that can move freely when the stopper of the flexible arm is off. The animal bed, which is made of a 2 mm thick plastic plate, is also supported by a flexible arm positioned on an X-Y-Z table. With these two flexible arms with the X-Y-Z table, we can position an animal quite freely and precisely.

2.3. Performance measurements

All performance measurements were carried out in an air-conditioned room outside of the MRI system.

2.3.1. Two-dimensional position histogram. Two-dimensional distribution was measured by uniformly irradiating 661 keV gamma photons of Cs-137 approximately 5 cm from the Si-PM block detector surface. Two-dimensional distribution was evaluated by setting the profiles

for the horizontal and vertical directions, and the peak-to-valley ratio was calculated for each direction.

2.3.2. Energy resolution and pulse shape spectra. The energy resolution was measured by setting the position boundaries on the two-dimensional distribution measure for the Cs-137 gamma source and plotting the energy spectra for 11 × 9 LGSO dual layer scintillators. We calculated the energy resolution for all these energy spectra; the average energy resolution was also calculated. The pulse shape spectra were derived from the same data and plotted for 11 × 9 LGSO dual layer scintillators. We calculated all peak-to-valley ratio as well as average peak-to-valley ratio.

2.3.3. Spatial resolution. The transaxial and axial resolutions of the PET system were measured using a Na-22 point source contained in a plastic container whose diameter was 1 mm. Measurements were made at the center and moved off-center with 5 mm steps. Images were reconstructed using filtered backprojection with a sharp filter. Reconstruction was performed with and without DOI correction. The DOI correction was performed by acquiring all four combinations of coincidence lines between two DOI layers and images were reconstructed using the depth information. The images without DOI correction were reconstructed after summing all combinations of DOI layers without any processing.

2.3.4. Sensitivity. The sensitivity profile was measured using a calibrated Na-22 point source by moving in an axial direction in 1 mm steps.

2.3.5. Count rate characteristics. The count rate performance was measured following the decay of the F-18 solution with activity of ~37 MBq (1 mCi) using a 30 mm diameter, 50 mm long cylindrical phantom.

2.3.6. Temperature-dependent sensitivity change of system. The temperature-dependent sensitivity change of the system was evaluated using a Na-22 point source positioned at the center of the field of view (FOV) of the detector ring. The count rate of the PET system and the room temperature were measured for 8 h. Temperature was measured by a thermometer (TZ-1CA-K22, Asahi Keiki Co., Tokyo).

2.3.7. Small animal imaging. Using the developed Si-PM PET, F-18-NaF rat brain imaging, F-18-FDG rat brain imaging and F-18-FDG mouse heart imaging were carried out. For the F-18-NaF rat brain imaging, approximately 37 MBq (1 mCi) F-18-NaF was injected, and the measurement was made for 20 min, from 2 h after the injection. For the F-18-FDG rat brain imaging, approximately 37 MBq (1 mCi) F-18-FDG was injected, and measurement was made for 20 min, from 4 h after the injection. For the F-18-FDG mouse heart imaging, approximately 37 MBq (1 mCi) F-18-FDG was injected, and the measurement was made for 30 min, from 4 h after the injection. All these data were reconstructed using filtered backprojection with moderate smoothing to reduce the image noise. In the mouse heart study, images were magnified by a factor of 2 in the reconstruction process because the size of the mouse heart was so small.

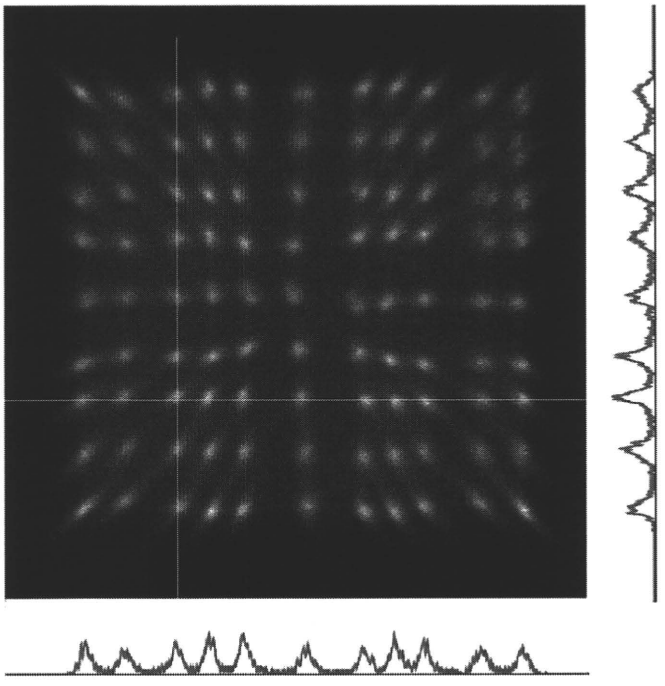

Figure 5. Two-dimensional distribution of the Si-PM-based block detector for 661 keV gamma photons.

3. Results

3.1. Two-dimensional position histogram

Two-dimensional distribution for the Si-PM block detector is shown in figure 5. All 11 × 9 LGSO scintillators are clearly resolved. The average peak-to-valley ratios for the horizontal and vertical lines were 9.7 and 11.7, respectively.

3.2. Energy resolution and pulse shape spectra

The energy spectrum for the LGSO scintillator with a single peak is shown in figure 6(A). Energy resolution ranged from 14% to 55%, and the average energy resolution was 27% FWHM. The pulse shape spectrum for one LGSO scintillator is shown in figure 6(B). The peak-to-valley ratio ranged from 1.1 to 1.9, and the average peak to valley ratio was 1.4.

3.3. Spatial resolution

We show the radial and tangential resolution as a function of distance from the center in figures 7(A) and (B), respectively. The spatial resolution at the center of the FOV was approximately 1.6 mm FWHM. Radial resolution using the DOI information (DOI) at 15 mm off-center was better than that without DOI information (nonDOI). The axial resolution at the center of the FOV was 1.3 mm FWHM.

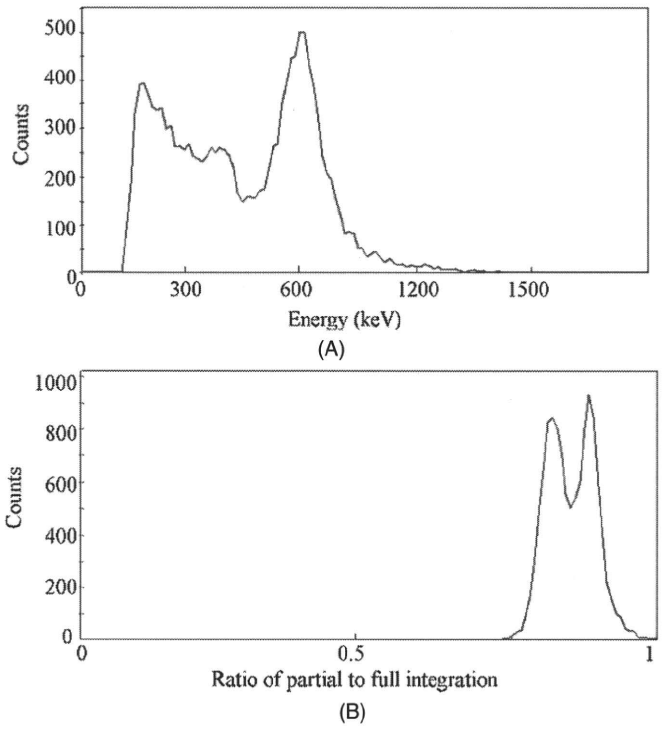

Figure 6. Energy spectrum (A) and pulse shape spectrum (B) of the Si-PM-based block detector for 661 keV gamma photons.

3.4. Sensitivity

The sensitivity profile as a function of the axial position is shown in figure 8. Sensitivity for the point source was 0.6% at the center of the axial FOV.

3.5. Count rate characteristics

The count rate characteristic is shown in figure 9. The maximum prompt minus delayed count rate was around 20 kcps. The small fluctuations of the count rates (approximately four cycles per 10 000 s) are due to the temperature-dependent sensitivity changes of the PET system.

3.6. Temperature-dependent sensitivity change of system

The temperature and the prompt minus delayed count rate measured over 8 h are shown in figure 10. The count rate was calculated by its running averages for 60 s to reduce the statistical variations. Due to the automatic on-and-off function of the air conditioner, the room temperature fluctuated between ~22 °C and ~23.5 °C, which is approximately three cycles per 7200 s. The count rate changed 9%, which is almost inversely proportional to the room temperature.

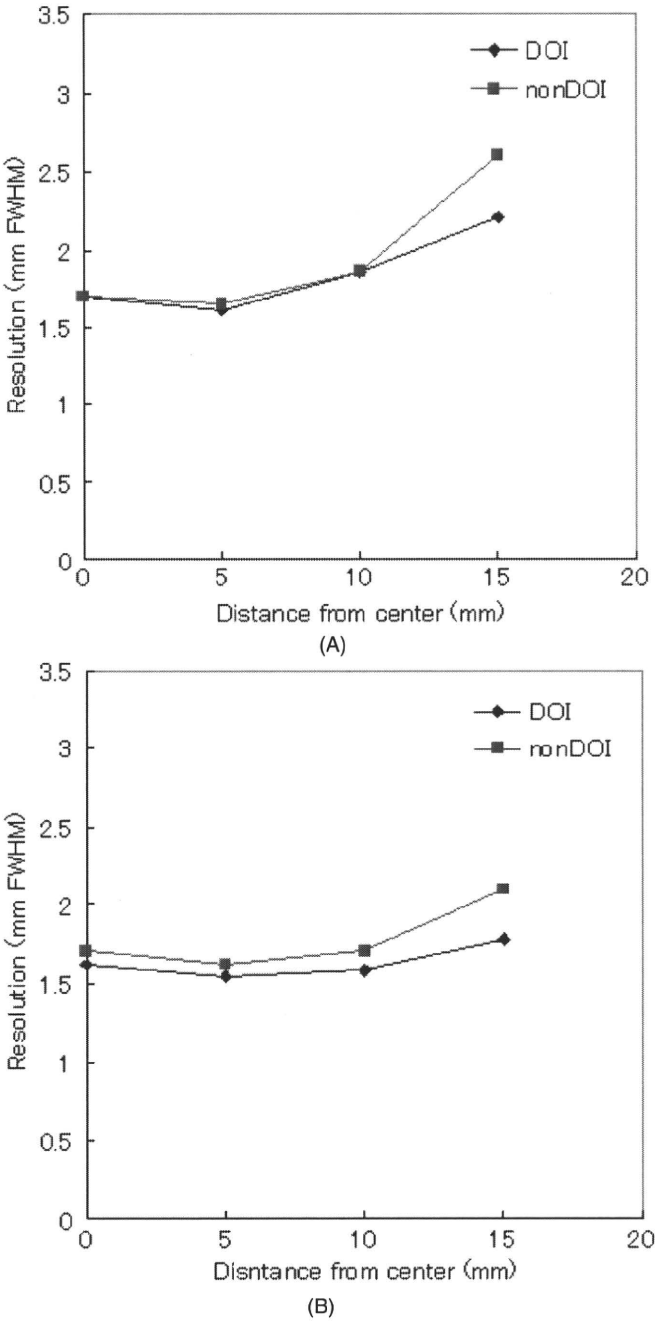

Figure 7. Radial (A) and tangential (B) resolution as a function of distance from the center. DOI is with depth-of-interaction correction by the software in reconstruction processing, and non-DOI is without depth-of-interaction information.

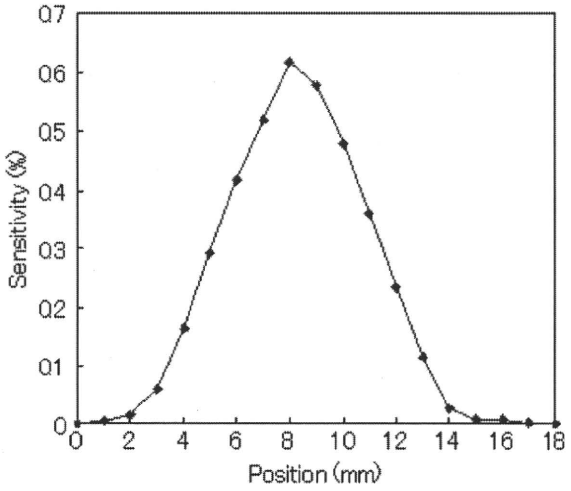

Figure 8. Sensitivity profile as a function of axial position.

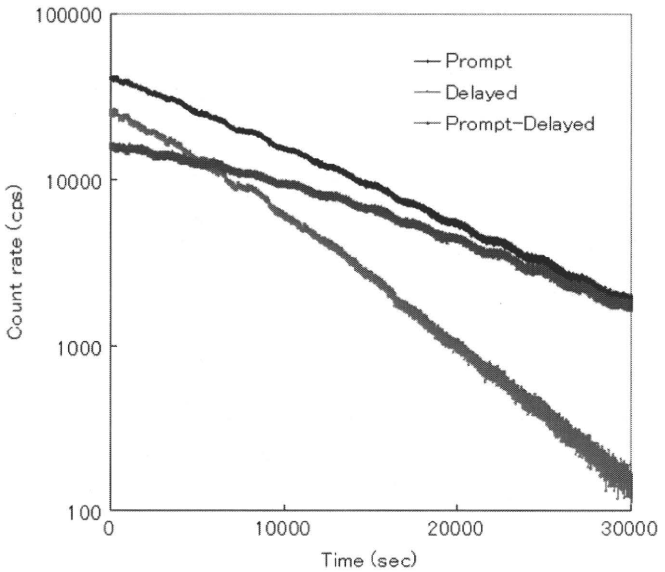

Figure 9. Count rate curve of the Si-PM PET system.

3.7. Small animal images

Images of an F-18-NaF study of a rat brain are shown in figure 11(A) in which the skull structure is clearly observed. Images of an F-18-FDG study of a rat brain are shown in figure 11(B) in which the cortex and thalamus structures are distinguished. Images of an F-18-FDG study of a mouse heart are shown in figure 11(C) in which the myocardial structure is observed.

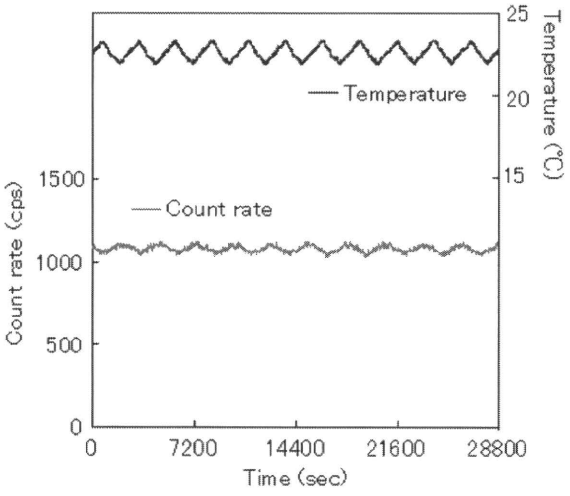

Figure 10. Temperature and count rate (prompt minus delayed) changes of the Si-PM PET system.

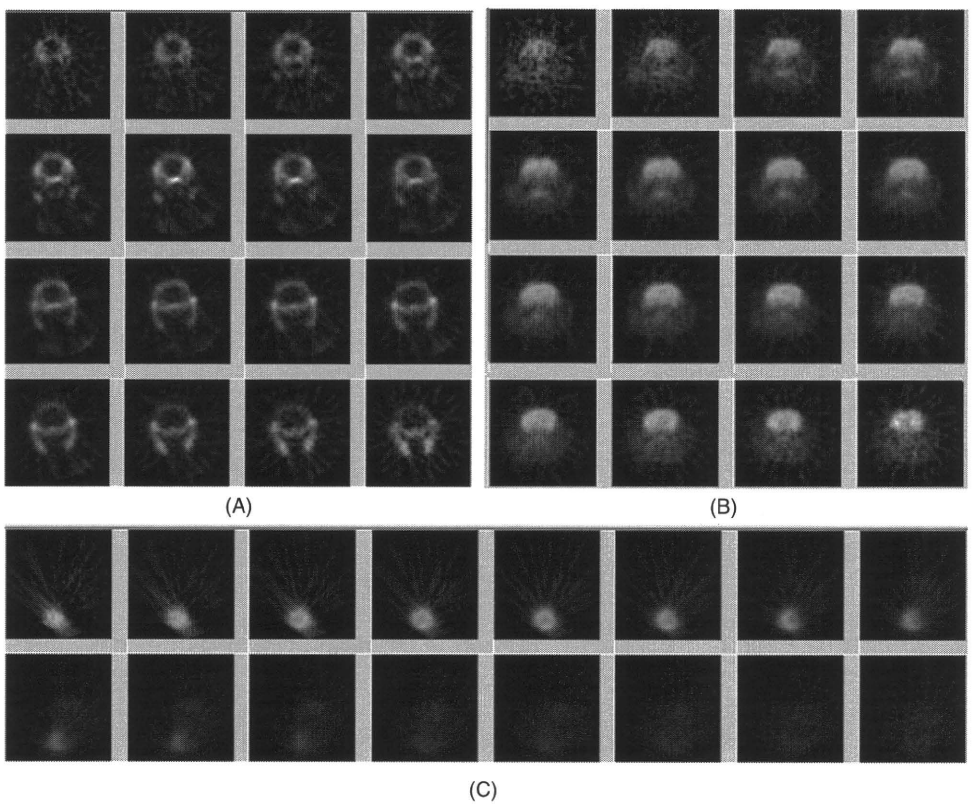

Figure 11. Images of the F-18-NaF study of the rat brain (A), the F-18-FDG study of the rat brain (B), and the F-18-FDG study of the mouse heart (C).

4. Discussion

We successfully developed a Si-PM-based PET system for small animals. One advantage of Si-PM-based systems over the conventional PMT or PSPMT-based PET systems is their compactness. The outside diameter of the detector ring of the Si-PM PET system is only 11 cm, which is much smaller than the PMT or PSPMT-based PET systems, because the electronics circuit was positioned outside the detector ring. Compared with the APD-based PET systems, the size of the detector ring is also small because an APD-based PET system needs to position an ASIC near the detector ring except for the APD-based PET detectors developed for PET/MRI systems that have a small diameter by positioning the ASIC side of the APD (Pichler *et al* 2006, Judenhofer *et al* 2008, Catana *et al* 2006, 2008). The small diameter of the developed Si-PM-based PET system will simplify its use in a narrow place such as inside the MRI tunnel.

Another advantage of the Si-PM-based PET system is its insensitivity to the static magnetic field, which makes it easy to use in a high magnetic field in MRI. In the developed Si-PM PET system, no electronics part (except a connector and a capacitor) was contained near the Si-PM-based block detectors. In addition, the analog signals from the Si-PM arrays are transferred to the front-end electronics using 1.2 m long small diameter coaxial cables. Because the developed Si-PM detector ring can be easily replaced from the plastic ring support, the detector ring can be set in the MRI tunnel quite easily. However more investigation on the interference between PET and MRI and such modifications as electrostatic shields may be needed for the use in MRI.

Compared with other small animal PET systems, the spatial resolution of the developed PET system (1.6 mm FWHM) was slightly worse than those with similar scintillator sizes (Tai *et al* 2003, 2005). For example, the spatial resolution of a small animal PET system that employed 1.5 mm LSO scintillators (Tai *et al* 2005) had 1.3 mm FWHM resolution at the center of the FOV. One reason for the inferior spatial resolution of the developed system is the relatively large size of the Na-22 point source used for the spatial resolution measurements (1 mm). Other reason is that such system parameters as lower energy threshold level were not optimized to obtain the best spatial resolution. The sensitivity of the developed system (0.6% at center) was much smaller than the other small animal systems (Tai *et al* 2003, 2005, Surti *et al* 2005) because of the small axial FOV. The explanation for the small axial FOV (11.7 mm) of the developed system is simply its cost consideration.

In the developed PET system, conventional filtered backprojection was used for the image reconstruction. Thus, the reconstructed small animal images measured by the developed PET system contained streaking noises in the low activity level especially at the edges of the axial from FOV. It may be possible to use model-based iterative reconstruction (Tohme and Qi 2009) to improve the quality of the reconstructed images as well as the performance of the developed PET system.

The energy resolution of the Si-PM-based block detector was not very good because the detector used a dual-layer LGSO configuration. More than 10% of the LGSO scintillators had double peaks in the energy spectra worsening the average energy resolution. The double peak may be caused by the photocoupling between the two types of LGSO blocks. However, by setting individual energy windows for each layer, the double peak problem can be solved.

The peak-to-valley ratio of the pulse shape spectra of the Si-PM-based block detector was not very good; the average peak-to-valley ratio was 1.4. One reason is the relatively slow fall time of the weighted sum signals probably due to the capacitance of the Si-PM arrays and the small diameter coaxial cables as well as the insufficient bandwidth of the weighted summing

amplifiers. Another reason may be a multiple interaction in the block detector; i.e., when Compton scattered gamma photons are detected in another layer, these events are positioned between peaks in the pulse shape spectra, degrading the peak-to-valley ratio.

The two-dimensional histogram showed good separation and wide margins between the spots of the scintillators. This indicates that much smaller scintillators can be used for the Si-PM-based block detectors, and a PET system with much higher spatial resolution can be realized by using the Si-PM array and LGSO or LYSO scintillators.

The Si-PM used for the block detector has high temperature-dependent gain. 1.5 °C temperature change produced 9% sensitivity change of the developed PET system. During the experiments presented in this paper, we did not observe any significant artifacts on the reconstructed images. However if used under more severe temperature conditions, a temperature-dependent gain control system may solve some of the temperature-related gain variation problems because circuits for the temperature-dependent gain control system are included in the developed front-end system. By calculating the correction factor for the temperature-dependent gain for the Si-PM arrays and compensating for the temperature-dependent gain, the Si-PM PET system will be more stable for a wide range of environmental conditions.

5. Conclusion

We developed a Si-PM-based PET system. The spatial resolution was 1.6 mm FWHM, and sensitivity was 0.6% at the center of the FOV. High-resolution mouse and rat images were successfully obtained. We confirmed that the developed Si-PM-based PET system is promising for small animal imaging. Using the developed Si-PM PET system, measurements inside MRI will be carried out in the near future, and an integrated PET/MRI system will be realized.

Acknowledgments

The authors thank Mr Ohta of Eiko-Sangyo for designing and manufacturing the mechanical part of the PET system. This work was partly supported by the Ministry of Education, Science, Sports and Culture, Japan, and the National Institute of Biomedical Innovation, Osaka, Japan.

References

Catana C *et al* 2008 Simultaneous *in vivo* positron emission tomography and magnetic resonance imaging *Proc. Natl Acad. Sci. USA* **105** 3705–10

Catana C, Wu Y, Judenhofer M S, Qi J, Pichler B J and Cherry S R 2006 Simultaneous acquisition of multislice PET and MR images: initial results with a MR-compatible PET scanner *J. Nucl. Med.* **47** 1968–76

Cuddy S, Reznik A, Rowlands J A and Taghibakhsh F 2010 Effect of scintillator crystal geometry and surface finishing on depth of interaction resolution in PET detectors—Monte Carlo simulation and experimental results using silicon photomultipliers *Proc. SPIE* **7622** 76221–8

Finocchiaro P, Pappalardo A, Cosentino L, Belluso M, Billotta S, Bonanno G and Mauro S D 2009 Features of silicon photo-multipliers: precision measurements of noise, cross-talk, after pulsing, detection efficiency *IEEE Trans. Nucl. Sci.* **56** 1033–41

Garlick P B *et al* 1997 PET and NMR dual acquisition (PANDA): applications to isolated, perfused rat heart *NMR Biomed.* **10** 138–42

Henseler D, Grazioso R, Nan Zhang and Schmand M 2009 SiPM performance in PET applications: an experimental and theoretical analysis *IEEE Nuclear Science Symp. and Medical Imaging Conf. (NSS/MIC)* pp 1941–8

Hong S J, Song I C, Ito M, Kwon S I, Lee G S, Sim K-S, Park K S, Rhee J T and Lee J S 2008 An investigation into the use of Geiger-mode solid-state photomultipliers for simultaneous PET and MRI application *IEEE Trans. Nucl. Sci.* **55** 882–8

Judenhofer M S *et al* 2008 Simultaneous PET-MRI: a new approach for functional and morphological imaging *Nat. Med.* **14** 459–65

Kolb A, Lorenz E, Judenhofer M S, Renker D, Lankes K and Pichler B J 2010 Evaluation of Geiger-mode APDs for PET block detector designs *Phys. Med. Biol.* **55** 1815–32

Llosáa G *et al* 2009a First results in the application of silicon photomultiplier matrices to small animal PET *Nucl. Instrum. Methods* A **610** 196–9

Llosáa G *et al* 2009b A Monolithic 64-channel SiPM matrices for small animal PET *IEEE Nuclear Science Symp. Medical Imaging Conf. (NSS/MIC)* pp 2658–61

Llosáa G *et al* 2009c Energy, timing and position resolution studies with 16-pixel silicon photomultiplier matrices for small animal PET *IEEE Trans. Nucl. Sci.* **56** 2586–93

Ottea A N *et al* 2005 A test of silicon photomultipliers as readout for PET *Nucl. Instrum. Methods* A **545** 705–15

Pichler B J, Judenhofer M S, Catana C, Walton J H, Kneilling M, Nutt R E, Siegel S B, Claussen C D and Cherry S R 2006 Performance test of an LSO-APD detector in a 7-T MRI scanner for simultaneous PET/MRI *J. Nucl. Med.* **47** 639–47

Raylman R R *et al* 2006 Simultaneous MRI and PET imaging of a rat brain *Phys. Med. Biol.* **51** 6371–9

Schaart D R, Seifert S, Vinke R, van Dam H T, Dendooven P, Löhner H and Beekman F J 2010 LaBr(3):Ce and SiPMs for time-of-flight PET: achieving 100 ps coincidence resolving time *Phys. Med. Biol.* **55** N179–89

Schaart D R, van Dam H T, Seifert S, Vinke R, Dendooven P, Löhner H and Beekman F J 2009 A novel, SiPM-array-based, monolithicscintillator detector for PET *Phys. Med. Biol.* **54** 3501–12

Shao Y *et al* 1997a Development of a PET detector system compatible with MRI/NMR system *IEEE Trans. Nucl. Sci.* **44** 1167–71

Shao Y *et al* 1997b Simultaneous PET and MR imaging *Phys. Med. Biol.* **42** 1965–70

Shimizu S *et al* 2006 Scintillation properties of Lu Gd SiO:Ce (LGSO) crystal *IEEE Trans. Nucl. Sci.* **53** 14–17

Slate R, Cherry S R, Boutefnouchet A, Shao Y, Dahlbom M and Farahani K 1999 Design of a small animal MR compatible PET scanner *IEEE Trans. Nucl. Sci.* **46** 565–70

Surti S, Karp J S, Perkins A E, Cardi C A, Daube-Witherspoon M E, Kuhn A and Muehllehner G 2005 Imaging performance of A-PET: a small animal PET camera *IEEE Trans. Med. Imaging* **24** 844–52

Tai Y C, Chatziioannou A F, Yang Y, Silverman R W, Meadors K, Siegel S, Newport D F, Stickel J R and Cherry S R 2003 MicroPET II: design, development and initial performance of an improved microPET scanner for small-animal imaging *Phys. Med. Biol.* **48** 1519–37

Tai Y C, Ruangma A, Rowland D, Siegel S, Newport D F, Chow P L and Laforest R 2005 Performance evaluation of the microPET focus: a third-generation microPET scanner dedicated to animal imaging *J. Nucl. Med.* **46** 455–63

Tohme M S and Qi J 2009 Iterative image reconstruction for positron emission tomography based on a detector response function estimated from point source measurements *Phys. Med. Biol.* **54** 3709–25

Yamamoto S 2008 Optimization of the integration time of pulse shape analysis for dual layer detector with different amount of Ce *Nucl. Instrum. Methods* A **587** 319–23

Yamamoto S *et al* 2009 A multi-slice dual layer MR-compatible animal PET system *IEEE Trans. Nucl. Sci.* **56** 2706–13

Yamamoto S, Imaizumi M, Kanai Y, Tatsumi M, Aoki M, Sugiyama E, Kawakami M, Shimosegawa E and Hatazawa J 2010 Design and performance from an integrated PET/MRI system for small animals *Ann. Nucl. Med.* **24** 89–98

Yamamoto S and Murayama H 2005 A block detector for a multi-slice depth of interaction MR-compatible PET *IEEE Trans. Nucl. Sci.* **52** 33–7

Yanagida T *et al* 2009 Development of Pr:LuAG scintillator array and assembly for positron emission mammography *IEEE Trans. Nucl. Sci.* **56** 10–16

IOP PUBLISHING PHYSICS IN MEDICINE AND BIOLOGY

Phys. Med. Biol. **55** (2010) 3813–3826 doi:10.1088/0031-9155/55/13/016

A compact and high sensitivity positron detector using dual-layer thin GSO scintillators for a small animal PET blood sampling system

Seiichi Yamamoto[1,5], Masao Imaizumi[2], Eku Shimosegawa[2], Yasukazu Kanai[2], Yusuke Sakamoto[3], Kotaro Minato[3], Keiji Shimizu[4], Michio Senda[4] and Jun Hatazawa[2]

[1] Kobe City College of Technology, Kobe, Japan
[2] Department of Nuclear Medicine and Tracer Kinetics, Osaka University Graduate School of Medicine, Osaka, Japan
[3] Nara Institute for Science and Technology, Nara, Japan
[4] Institute for Biological Research and Innovation, Kobe, Japan

E-mail: s-yama@kobe-kosen.ac.jp

Received 11 November 2009, in final form 21 May 2010
Published 15 June 2010
Online at stacks.iop.org/PMB/55/3813

Abstract

For quantitative measurements of small animals such as mice or rats, a compact and high sensitivity continuous blood sampling detector is required because their blood sampling volume is limited. For this purpose we have developed and tested a new positron detector. The positron detector uses a pair of dual-layer thin gadolinium orthosilicate (GSO) scintillators with different decay times. The front layer detects the positron and the background gamma photons, and the back layer detects the background gamma photons. By subtracting the count rate of the latter from that of the former, the count rate of the positrons can be estimated. The GSO for the front layer has a Ce concentration of 1.5 mol% (decay time of 35 ns), and that for the back layer has a Ce concentration of 0.5 mol% (decay time of 60 ns). By using the pulse shape analysis, the count rate of these two GSOs can be discriminated. The thickness is 0.5 mm, which is thick enough to detect positrons while minimizing the detection of the background gamma photons. These two types of thin GSOs were optically coupled to each other and connected to a metal photomultiplier tube (PMT) through triangular light guides. The signal from the PMT was digitized by 100 MHz free-running A-D converters in the data acquisition system and digitally integrated at two different integration times for the pulse shape analysis. We obtained good separation of the pulse shape distributions of these two GSOs. The energy threshold level was decreased to 80 keV, increasing the sensitivity of the detector. The sensitivity of a small diameter plastic tube was 8.6% and 24% for the F-18 and C-11 positrons, respectively. The

[5] Author to whom any correspondence should be addressed

0031-9155/10/133813+14$30.00

count rate performance was linear up to ~50 kcps. The background counts from the gamma photons could be precisely corrected. The time–activity curve (TAC) of the rat artery blood was successfully obtained and showed a good correlation with that measured using a well counter. With these results, we confirmed that the developed blood sampling detector is promising for quantitative measurement for an animal positron emission tomography system.

1. Introduction

Continuous blood sampling for quantitative measurement of animal positron emission tomography (PET) studies from such small animals as mice or rats is difficult because their blood sampling volume is limited (McGuill and Rowan 1989, Morton 1993). To minimize the amount of blood, a small diameter tube must be used for detecting the positrons or annihilation gamma photons from the animal blood in the tube. However, when a small diameter tube is used, the count rate decreases and statistical deviation increases since the count rate of the blood sampling detector is proportional to the amount of blood in the tube.

To solve these problems, several approaches were reported to measure the input function without blood sampling. One is dynamic imaging of blood pool of the heart of a mouse or a rat using an animal PET scanner to obtain the image-based input function (Kim *et al* 2006, Ferl *et al* 2007, Su *et al* 2007). However, these image-based techniques are not easy to implement due to the small size of the heart of these small animals and the limited spatial resolution of most small animal PET systems. The other approach is using an intra-blood-vessels probe for the measurement of an input function (Pain *et al* 2004). Although these approaches have their advantages, the reliability of the input function must be validated by comparing with the blood sampling data.

To measure the continuous blood sampling curve in good statistics, a high sensitivity blood sampling detector is needed. In addition, the distance from the animal to the blood sampling detector must be small to shorten the blood sampling tube to minimize the amount of blood.

A positron emitter can be detected by two methods for blood sampling detectors. One is the detection of positrons (beta particles) from the blood in the tube (Hutchins *et al* 1986, Convert *et al* 2007). The drawback of this method is that its sensitivity is relatively low because a high energy threshold level must be set to minimize the detection of the 511 keV gamma photons from outside the tube such as the syringe or the animal's body. The energy threshold is usually set above 511 keV to minimize the detection efficiency of these background annihilation gamma photons. A suitable radionuclide for this positron detector is O-15 because of its high positron energy. To overcome these limitations, a phoswich positron detector for a blood sampling system was developed (Yamamoto *et al* 2001). The positron detector, which consists of a plastic scintillator and a bismuth germanate (BGO) scintillator, measures beta-gamma coincidence between these two scintillators to detect only positrons. By using the beta-gamma coincidence, the energy threshold was lowered and sensitivity could be increased. However, the detector remained too big because the BGO scintillator was relatively large, and a thick gamma shield was needed to reduce the gamma photons from outside the tube.

The other method for continuous blood sampling detectors is the coincidence measurement of annihilation gamma photons (Eriksson *et al* 1988, Votaw and Shulman 1998, Kudomi *et al* 2003). The detectors employed two BGO or GSO detectors and measured the coincidence between the annihilation photons from the blood in the tube. The advantage of this method

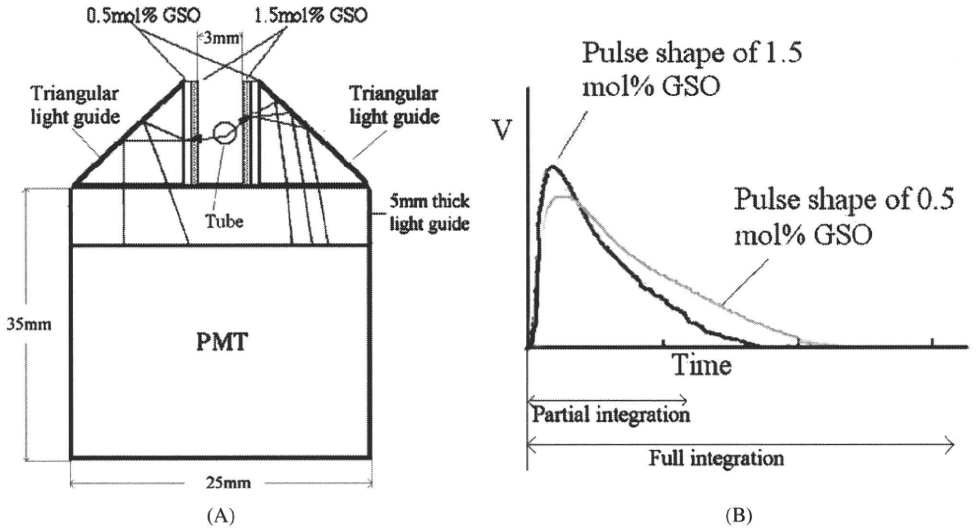

Figure 1. Schematic drawings of the developed positron detector (A) and the schematic pulse shape of 1.5 mol% Ce: GSO and that of 0.5 mol% Ce: GSO (B).

is that the sensitivity does not depend on the positron energy, and a low energy positron radionuclide such as F-18 can be measured. However, to achieve high sensitivity, large scintillators must be used. In addition, a thick gamma shield is needed to reduce the gamma photons from outside the tube to minimize accidental coincidence events. Consequently, developing a compact and high-sensitivity blood sampling detector is difficult using this coincidence method. To overcome these limitations, we developed a blood sampling detector based on a new concept. Our developed blood sampling detector has high sensitivity, small size and is suitable for animal PET studies.

2. Materials and methods

2.1. Principle of detector operation

The blood sampling detector is based on a positron detector with gamma photon rejection capability. A schematic drawing of the developed detector is shown in figure 1(A). The detector consists of a pair of thin GSO scintillators whose Ce concentrations are 1.5 mol% and 0.5 mol%, a pair of triangular light guides and a photomultiplier tube (PMT). The GSO scintillator usually dopes the Ce to increase its light output, and the decay times can be controlled by the concentration of the Ce (Ishibashi *et al* 1989, Yamamoto and Ishibashi 1998, Yamamoto 2008a). The GSO scintillators are optically coupled to the inner sides of the light guides, which are optically coupled to the PMT through a 5 mm thick light guide. We used GSO scintillators for separately detecting positrons (beta particles) from a tube and 511 keV gamma photons from outside the detector (background gamma photons). The front layer GSO scintillators detect the positrons and the background gamma photons, and the back layer GSO scintillators detect only the background gamma photons because the front layer GSO is thick enough to absorb all the positrons from the tube. For the separation of the count rate of the first- and second layer events, pulse shape analysis is used because the decay times of the GSO scintillators of 1.5 mol% Ce and 0.5 mol% Ce are different (figure 1(B)). By subtracting the

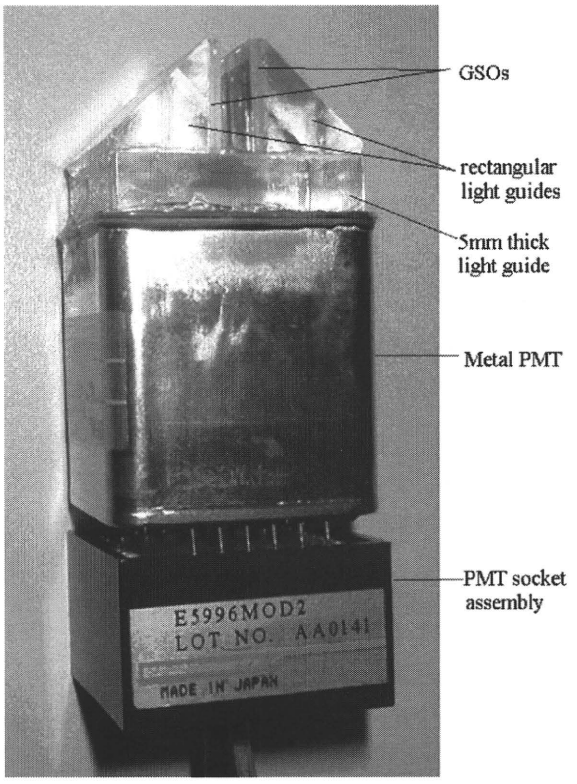

Figure 2. Photograph of the positron detector without the shield.

count rate of the back layer from that of the front layer, the count rate of the positrons can be estimated.

The scintillation photons produced in the GSO scintillators are fed to the triangular light guides that transfer the scintillation light to the PMT, which converts the scintillation light to an electric signal to be fed to the data acquisition system. In the data acquisition system, the pulse height and pulse shape discrimination are processed, and the count rates for the front and back layers are displayed and stored in the memory.

2.2. Developed blood sampling detector

Figure 2 shows the developed blood sampling detector without light or gamma shields. The GSO for the front layer has a Ce concentration of 1.5 mol% (decay time of 35 ns) and 0.5 mol% (decay time of 60 ns) for the back layer. The thickness of these GSOs is 0.5 mm, which is enough to detect the positrons and minimize the detection of the background photons (Knoll 1997). The GSO scintillators are 10 mm high and 20 mm wide. These two types of thin GSOs were optically coupled to each other using silicon rubber (Shin-etsu Silicone, KE-420, Tokyo, Japan) and connected to a 1 inch square metal photomultiplier tube (PMT: Hamamatsu Photonix, R-7600-U, Hamamatsu, Japan) through triangular light guides and a 5 mm thick light guide made of acrylic resin. The metal PMT was selected because the height of the tube is small and the size of the detector can be reduced. The 5 mm thick light guide was used to reduce

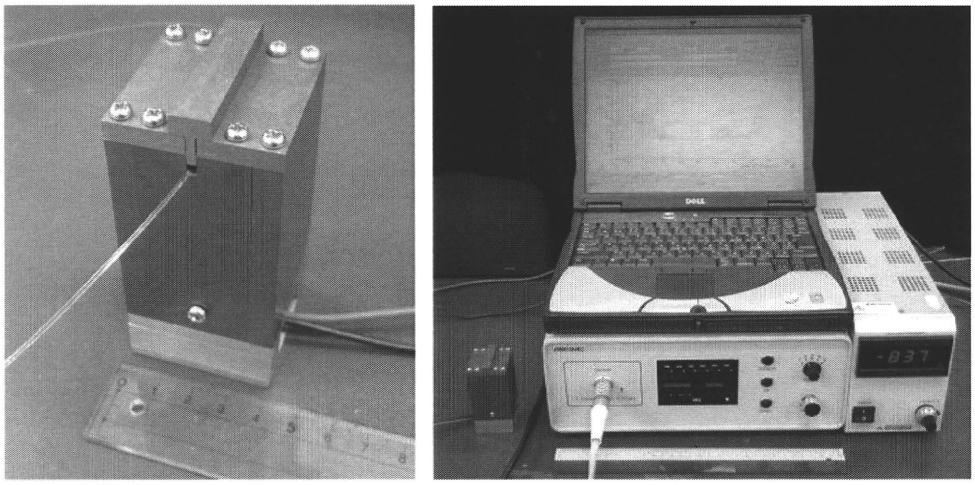

(A) (B)

Figure 3. Detector part (A) and blood sampling detector system composed of detector (left-hand side), electronics (middle lower), high voltage supply (right-hand side) and personal computer (middle upper) (B).

the non-uniformity of the photo-cathode sensitivity of the PMT. The gap between two pairs of these GSO scintillators was 3 mm. The signal from the PMT was digitized by 100 MHz free-running A-D converters in the data acquisition system and digitally integrated in two different integration times (120 ns for partial integration and 320 ns for full integration) for the pulse shape analysis. The pulse shape spectrum was digitally calculated from the ratio of these two integrated signals (Yamamoto 2008b). The energy spectrum was derived from the full integration signals (320 ns).

Figure 3(A) shows the blood sampling detector contained in a gamma shield. The detector in figure 2 was light shielded by black tape except for the surfaces of the GSO scintillators. The GSO scintillator surfaces were covered with three layers of aluminized Mylar film of whose aluminum thickness was $\sim$1 μm for the light shield to minimize the absorption of the beta particles (positrons). In the upper side of the gamma shield, a 2.5 mm wide slit was cut where a small diameter polystyrene tube (PE-10: inner diameter: 0.28 mm, outer diameter: 0.61 mm, Hagitec, Ciba, Japan) was positioned. The slit was cut so that the tube could be positioned at the center of the GSO scintillators to obtain the highest sensitivity. The tube was suspended between the GSO scintillators by taping the tube at the slits of the gamma shield. The gamma shield was made of a 4 mm thick tungsten alloy. The thickness of the gamma shield was selected to reduce the annihilation gamma photons $\sim$50% while minimizing the size of the blood sampling detector. The dimensions of the detector with the shield are 4 cm (width) $\times$ 4 cm (depth) $\times$ 8 cm (height) and it weighs 1.2 kg. After the tube was set, a T-shaped tungsten cap was placed in the slit of the gamma shield.

A photograph of the entire system of the blood sampling detector with a 30 cm long ruler is shown in figure 3(B). The system consists of the detector, data acquisition electronics, high voltage power supply and a notebook personal computer (PC). The signal from the detector is fed to the data acquisition electronics and the PC. The count rates for the front layer (positron + gamma), the back layer (gamma) and the front layer minus back layer (positron) are displayed on the monitor of the PC. Also these count rate curves are displayed on the monitor. The